No extraordinary $\chi^{(3)}$ in lead-halide perovskites: placing an upper bound on Kerr nonlinearity by means of time-resolved interferometry

Dusan Lorenc,[1,2] Ayan Zhumekenov,[3] Osman M. Bakr,[3] and Zhanybek Alpichshev[1,*]

[1]*Institute of Science and Technology Austria, Am Campus 1, 3400 Klosterneuburg, Austria*

[2]*International Laser Centre, Ilkovicova 3, 84104 Bratislava, Slovakia*

[3]*KAUST (King Abdullah University of Science and Technology), Thuwal 23955, Saudi Arabia*

(Received 22 December 2023; accepted 30 July 2024; published 23 August 2024)

Lead halide perovskites have recently been reported to demonstrate an exceptionally high nonlinear (Kerr) refractive index n_2 of up to 10^{-8} cm^2/W in $CH_3NH_3PbBr_3$. Other researchers, however, observe different, substantially more conservative numbers. In order to resolve this disagreement, the nonlinear Kerr index of a bulk sample of lead halide perovskite was measured directly by means of an interferometer. This approach has many advantages as compared to the more standard z-scan technique. In particular, this method allows studying the induced changes to the refractive index in a time-resolved manner, thus enabling to separate the different contributions to n_2. The extracted n_2 values for $CsPbBr_3$ and $MAPbBr_3$ at $\lambda \approx 1$ μm are $n_2 = +2.1 \times 10^{-14}$ cm^2/W and $n_2 = +6 \times 10^{-15}$ cm^2/W, respectively. Hence, these values are substantially lower than what has been indicated in most of the previous reports, implying the latter one should be regarded with great care.

DOI: 10.1103/PhysRevMaterials.8.085403

I. INTRODUCTION

Lead halide perovskites (LHPs) remain at the forefront of a number of research areas, including but not limited to: photovoltaics, material- and condensed matter- physics and photonics, where LHPs were recently demonstrated to exhibit remarkable nonlinear optical properties (see, e.g., [1–3]). In the specific case of lead-bromide perovskites $APbBr_3$, a significant Kerr nonlinearity as high as $n_2 \sim 10^{-8}$ cm^2/W [4–10] was reported, potentially making these compounds some of the most nonlinear bulk materials known to date. If confirmed, this can position LHPs as the future material of choice for $\chi^{(3)}$ nonlinear applications [3]. However, in addition to these reports of extreme Kerr indices, there are also works that report much more conservative numbers for Kerr nonlinearity in that lead-bromide perovskites $n_2 \sim 10^{-14}$ cm^2/W [11].

There are well-known reproducibility issues in perovskite research [12], but such orders-of-magnitude discrepancies across results obtained on nominally identically materials, such as $CH_3NH_3PbBr_3$, imply that it is rather unlikely that the source of the variance in magnitude of nonlinearity is purely due to actual intrinsic material properties of respective LHP samples used in the studies.

Besides material properties, the only remaining source of disagreement among Kerr index reports would be the variance in experimental details in different works, such as the character of light sources used and the geometries of the samples. It is important in this regard to mention that, to the best of our knowledge, the majority of the n_2 values in LHPs reported so far were obtained via the so-called z-scan technique [3]. This method was developed in the early 1990s and has since established itself as a default tool of choice for measuring Kerr index in bulk materials [13]. The technique relies on the fact that space-dependent local intensity of the probe beam via Kerr effect gives rise to a space-dependent local refractive index distribution inside the sample. Such profile manifests itself as a distortion of the wave-front of the probing beam. By modifying the intensity distribution of the probe and monitoring the effects on the probe beam, one can, in principle, deduce the value of the Kerr index. Specifically, in z-scan the local intensity profile is modified by moving the sample along the beam direction through the focal region of the probe. The biggest merit of this method, which has warranted its popularity, is its simplicity both in terms of experimental infrastructure and theoretical analysis. However, the description of the z-scan above also highlights the typical issues that one can face when employing this method. Firstly, since at different stages of the measurement different parts of the sample are illuminated, the local geometry of the sample and its optical uniformity along with the properties of the pump beam become crucial [14,15]. Secondly, and most importantly, z-scan is essentially a static method that measures the integrated effect of the probing beam on the refractive index of the sample. In particular, in addition to the narrowly defined quasi-instantaneous "intrinsic" electronic Kerr effect, z-scan also picks up refractive index modifications due to "extrinsic" phenomena, such as electrosctriction, thermo-optic and photo-refractive effects.

As it turns out, many of these issues are featured prominently in lead-halide perovskites. In particular, they have been demonstrated to exhibit strong photo-refractive and electrostrictive effects [16,17]. Thermo-optic corrections to the refractive index were also found to be featured prominently in LHP samples [18], which becomes of particular concern given the exceptionally poor heat conductivity of these materials [19]. The main problem here is that extrinsic contributions to the Kerr response are orders of magnitude stronger than the electronic one [20,21], making it challenging to extract the intrinsic nonlinear refractive index of the medium from

*Contact author: alpishev@ist.ac.at

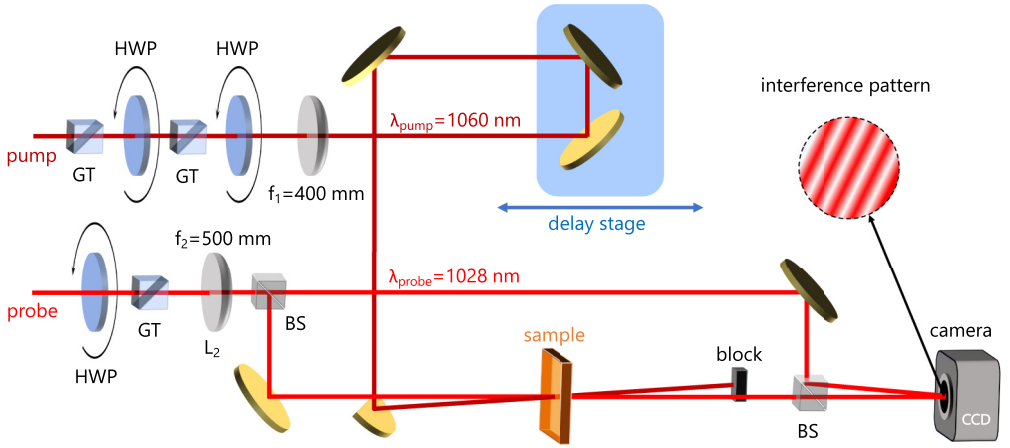

FIG. 1. Schematic layout of the time-resolved Mach-Zehnder interferometer (MZI). Pump and probe beams are near-degenerate ($\lambda =$ 1060 nm and 1028 nm, respectively). Transient pump-induced changes in the refractive index are detected as shifts in the interference pattern recorded by a CCD camera.

studying the self-interaction of a light beam under general circumstances. To account for this, it is conventional to perform experiments using ultrafast laser pulses and make use of the quasi-instantaneous nature of the electronic response. The works that implement z-scan measurements typically check for fluence/repetition rate dependence of their z-scan signals [22] in order to decouple long-lived extrinsic effects from the instantaneous intrinsic ones, however this only works when the unwanted phenomena occur at timescales comparable to the typical pulse-repetition period. When the extrinsic effects persist for significantly longer than the longest interval between pulses, it is not always possible to isolate the instantaneous response (for instance, the photorefractive effect may have a response time on the order of tens of seconds).

Here, we circumvent the complications associated with z-scan measurements of the intrinsic (instantaneous) nonlinear Kerr index in LHP by means of measuring n_2 in a time-resolved fashion. To this end, we measure the nonlinear corrections to the refractive index directly by means of interferometry. As will be demonstrated below, such approach has a number of advantages as compared to the classic z-scan method: 1) the setup remains static throughout measurement (i.e., sample is not being moved), therefore the method is insensitive to the irregularities of the geometry and the inner inhomogeneities of the sample; 2) the average incident power on the sample remains the same throughout the experiment with the heating, due to radiation, thus only affecting the effective sample temperature; 3) studying transient changes of the refractive index in real time allows separating different contributions to the nonlinear response; 4) pump and probe are separate beams whose polarizations can be controlled independently; 5) by not being dependent on sample homogeneity, the proposed approach allows measuring on bulk single-crystal samples. This has the advantage of minimizing the possible size effects in nanocrystals and to focus on the intrinsic properties of the material. Note that our goal was to establish a reliable order of magnitude estimate on the n_2 of the respective perovskites rather than providing an exact analysis of the magnitude of Kerr nonlinearity.

II. EXPERIMENT

In optical Kerr effect, the (phase) refractive of the medium is modified in the presence of radiation with intensity I according to $n(I) = n_0 + n_2 I$ with n_0 and n_2 referred to as linear and nonlinear (Kerr) refractive indices, respectively. While it is often the case that I is the intensity of the very beam that also "experiences" the refractive index n (self-phase modulation), it does not always have to be so. In this work, to study the Kerr effect in a time-resolved manner we use two separate laser beams. The first, more intense beam (the pump) is used to provide the intensity I to modify the refractive index of the medium, while the other beam (the probe) is used to probe the resulting refractive index. Since Kerr-induced changes $\Delta n = n_2 I$ are usually weak for generic materials, we choose to detect them here by resorting to interferometry.

The experimental layout is schematically shown in Fig. 1. It consists of a Mach-Zehnder interferometer where the refractive index n of a sample put into one of the arms is modified by the pump beam. This change in n results in the change of the optical length of the corresponding arm of MZI, which manifests itself as a shift in the interferogram recorded by a CCD camera located at the exit of MZI. The delay between the pump and probe pulses can be controlled by a fast motorized delay stage (here, the Newport LTLMS800). To extract the time dependence of transient changes to n, the stage is moved incrementally and an interferogram is recorded for each position of the stage. In order to avoid the detrimental effect of mechanical vibrations, for every delay stage position we record two consecutive intefrograms: one at the actual desired position and the other at a fixed reference position predating pump arrival. The actual phase shift is then recorded as the difference in position of the interferogram relative to the one taken at the reference position. Together with the high speed of the delay stage (500 mm/s) this method helps minimize the effect of the low frequency noise coming from mechanical deformations of MZI. Each interferogram is then processed using a 2D fast Fourier transform and subsequently evaluated in order to extract the corresponding amplitude and phase (see Figs. 2(b) and 2(c)).

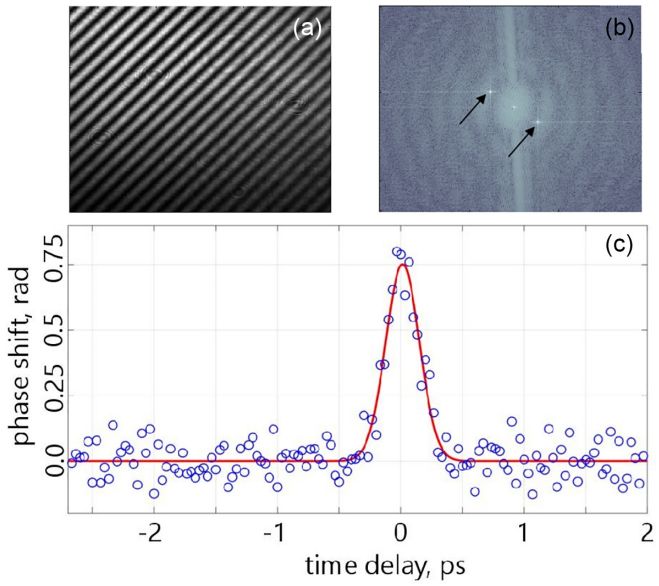

FIG. 2. (a) Sample interferogram as recorded by CCD camera; (b) 2D Fourier intensity of the interferogram. The real-space shift of the interference pattern is inferred from the change of the phase of complex amplitude at the peak. Time dependence of the pump-induced phase shifts between the two probe beams in MZI; (c) Pump-induced transient phase shift of the interference pattern in single crystal $CsPbBr_3$ taken with a pump pulse with peak intensity $I_0 = 3 \times 10^9\,\mathrm{W/cm^2}$. Solid red line is fit to a gaussian curve to extract the peak value of the phase shift $\Delta\phi$ at this pump intensity.

An amplified femtosecond laser system (here, the Light Conversion PHAROS) coupled to an optical parametric amplifier (OPA; here, the Light Conversion ORPHEUS) is used as the principal laser source. The laser produces a train of pulses centered at 1028 nm with a repetition rate of 3 kHz, a pulse duration of 300 fs, and a pulse energy of 2 mJ. A small part of the beam (5%) has been coupled into the Mach-Zehnder interferometer (MZI) through a variable attenuator consisting of a half-wave plate (HWP) and a Glan-Taylor polarizer, while the remaining part pumped the OPA (tuned between 0.66 and 16 μm). In this work, the fundamental wavelength of 1028 nm was used as a probe, while the 1060 nm idler output has been used as the pump radiation. The pump wavelength was chosen so as to be nearly degenerate with the probe, but still different enough to be effectively separable. The delay between pump and probe is controlled with a linear stage. Both pump and probe are passed through half-wave plates (HWP) and polarizers to attenuate their respective powers and to clean the polarizations. The pump beam then passes another free standing HWP in order to set its polarization state. The pump and probe beams were loosely focused and overlapped in the sample in a slightly noncollinear arrangement. Care was taken to make sure that the probe diameter inside of the sample was considerably smaller than that of the pump. This is to ensure that pump intensity is a well defined quantity. The probe light leaving the output port of MZI passed through a 1030 ± 5 nm bandpass filter and the resulting interferograms were recorded by a CCD camera (here, the Point Grey Research Inc. CM3-U3-50S5M). The pump intensity is tunable in a broad range while the probe intensity was kept fixed at $I_{\mathrm{probe}} = 4 \times 10^6\,\mathrm{W/cm^2}$. High quality bulk single crystal samples of $CH_3NH_3PbBr_3$ with a thickness of 1.72 mm were grown by the inverse temperature crystallization method, as described elsewhere [23,24] and similarly high quality bulk single-crystal samples of $CsPbBr_3$ with a thickness of 0.84 mm were grown by antisolvent vapor-assisted crystallization method as described in [25]. All experiments were performed at room temperature i.e., in the orthorhombic phase of $CsPbBr_3$ and cubic phase of $MAPbBr_3$.

III. RESULTS AND ANALYSIS

Figure 2(c) shows a sample trace of the transient phase shift as a function of pump-probe delay for the $CsPbBr_3$ sample taken at peak pump intensity $I_0 = 3 \times 10^9\,\mathrm{W/cm^2}$. The first thing to notice here is that the temporal-width of the signal is comparable to pulse-width of the pump pulse ($\tau \approx 270$ fs), meaning that the phase response can be considered instantaneous, and can therefore be fully ascribed to the intrinsic electronic hyperpolarizability of the medium. Having established the nature of the response this way, we can use the data to determine the numeric value of the intrinsic Kerr nonlinear index n_2. To this end, however, one needs to establish a relation between the measured peak phase shift $\Delta\phi_0$ and the Kerr-induced change in refractive index $\Delta n = n_2 I_0$. Based on scaling considerations, it is clear that one can write

$$\Delta\phi_0 = \gamma \times n_2 I_0\, 2\pi L/\lambda, \tag{1}$$

where L and λ are the thickness of the sample and probe wavelength, respectively; I_0 is the peak intensity with an unknown coefficient $\gamma \lesssim 1$ whose exact value depends on the particular details of pump and probe pulse temporal profiles ($\gamma = 1$ in the limit $I_{\mathrm{pump}}(t) = I_0$; see Figs. 3(a) and 3(b)). To estimate the value of γ we simulate the Kerr-interaction between the pulses by means of numerically integrating a system of coupled generalized nonlinear Schroedinger equations (CGNLSE) for frequency-nondegenerate fields [26]:

$$\begin{aligned}
&\frac{\partial A_1}{\partial z} + \frac{1}{v_{g1}}\frac{\partial A_1}{\partial z} + i\frac{\beta_{21}}{2}\frac{\partial^2 A_1}{\partial z^2} = i\Gamma_1(|A_1|^2 + 2|A_2|^2)A_1,\\
&\frac{\partial A_2}{\partial z} + \frac{1}{v_{g2}}\frac{\partial A_2}{\partial z} + i\frac{\beta_{22}}{2}\frac{\partial^2 A_2}{\partial z^2} = i\Gamma_2(|A_2|^2 + 2|A_1|^2)A_2.
\end{aligned} \tag{2}$$

Here A_j stands for the field amplitude of jth beam ($j = 1, 2$ for pump and probe beams, respectively); v_{gj} for the corresponding group velocities and β_{2j} are the GVD coefficients. These parameters can be extracted from refractive index measurements in these compounds [27–29]. Finally, Γ_j are the third-order nonlinear parameters that determine $n_2 = \Gamma_j\,\lambda_j S^j_{\mathrm{eff}}/2\pi$ withλ_j denoting the wavelength of the corresponding beam and S^j_{eff} being its effective diameter as defined in [26]. The reasons we were able to apply the simplified model (2) are threefold. First, the geometry considerations favor low phase-shifts within the sample, as detailed in the Supplemental Materials [30]. Second, the probe beam spatial profile at high pump intensities shows only modest distortions as depicted in Fig. 1 of the Supplemental Material [30] and no signatures of either beam collapse or sub-/super-structure. Third, the corresponding overall shift of the interference pat-

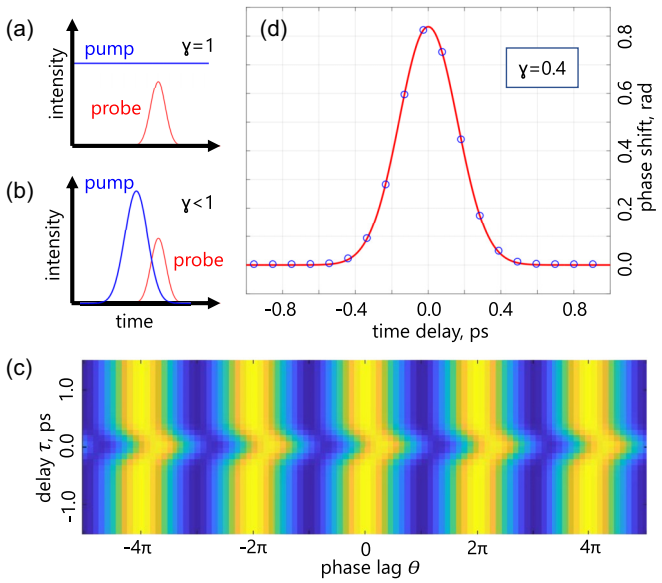

FIG. 3. (a) Default Kerr-effect configuration: the pump intensity is constant, and $\gamma = 1$ (see text); (b) experimental configuration with pulse-shaped pump and probe profiles. Different parts of the probe pulse experience different instantaneous pump intensity $I(t) \leqslant I_0$, therefore $\gamma < 1$; (c) CGNLSE-simulated interference pattern as a function of pump-probe delay τ calculated for $CsPbBr_3$ at $I_0 = 3 \times 10^9$ W/cm^2 and $n_2 = +2.1 \times 10^{-14}$ cm^2/W; and (d) pump-induced phase shift of interference pattern extracted from (c) versus delay τ (blue dots) and a Gaussian fit to it (red line).

tern as seen in Figs. 2 and 3 of the Supplemental Material is equally modest and no distortions of the interference fringes is observable. Hence we could safely drop the transverse spatial dependence of A_j and only consider the 1D case.

In order to relate the resultant pump-modified probe field amplitude $A_p(\tau, t)$ at the exit of the sample calculated for pump-probe delay τ to the experiment, we interfere it with a reference field $A_0(t)$ (calculated by integrating the same system of equations Eq. (2) with pump intensity put equal to zero) and calculate the resulting intensity:

$$F(\theta, \tau) = \int_{-\infty}^{+\infty} [A_p(\tau, t)A_0^*(t)e^{i\theta} + A_p^*(\tau, t)A_0(t)e^{-i\theta}]dt.$$

Here we introduce phase lag θ between the two fields. This quantity $F(\theta, \tau)$ above has the meaning of being proportional to the net average power resulting from the interference between the probe and reference beams as a function of phase lag θ between the interferometer arms and pump-probe delay τ. By calculating $F(\theta, \tau)$, one can simulate the Kerr-induced shift of the interference pattern, as shown in Fig. 3(c). Tracing the position of maximum of $F(\theta, \tau)$ as a function of τ for given n_2 and I_0, and comparing the peak phase shift $\Delta\phi$ with Eq. (1), we find that for the parameter values of our experiment $\gamma_{Cs} \approx 0.4$ for $CsPbBr_3$ and $\gamma_{MA} \approx 0.7$ for $MAPbBr_3$.

By using these values of γ, we can now convert phase shifts $\Delta\phi$ to refractive index changes Δn and plot the peak values of the latter as a function of peak pump intensity I_0 for both $CsPbBr_3$ and $MAPbBr_3$ as shown in Fig. 4. Note that all intensity values were corrected for Fresnel losses at the sample interface. To characterize the nonlinear Kerr effect in our LHP samples, we probe it in two configurations where pump and probe polarizations were kept parallel ("xx") and crossed ("xy") with respect to each other; in both cases, the polarization planes are aligned with the crystal axes. Here we can see that refractive index follows linear dependence $n(I) = n_0 + n_2 I$. From these fits we obtain for $CsPbBr_3$ $n_2^{xx} = (2.1 \pm 0.2) \times 10^{-14}$ cm^2/W (pump and probe polarizations parallel) and $n_2^{xy} = (5.5 \pm 0.2) \times 10^{-15}$ cm^2/W (crossed polarizations). For $MAPbBr_3$ we obtain $n_2^{xx} = (6.0 \pm 0.2) \times 10^{-15}$ cm^2/W and $n_2^{xy} = (3.3 \pm 0.1) \times 10^{-15}$ cm^2/W. These numbers are rather modest in comparison to some of the previous reports of n_2 in LHPs [3]. On the other hand, by the order of magnitude, they nicely fall into the range expected for generic semiconductors with comparable band gap, such as ZnSe [31–33]. Moreover, we have established a positive sign for the Kerr nonlinearity, meaning the obtained values represent an upper limit on the magnitude as any unaccounted-for Kerr lensing would only increase the intensity inside of the sample, thereby resulting in a decrease of evaluated n_2 value.

IV. CONCLUSION

In summary, we measured the intrinsic nonlinear (Kerr) refractive index n_2 of a bulk single crystal $CsPbBr_3$ and $MAPbBr_3$. Given the orders-of-magnitude variance among

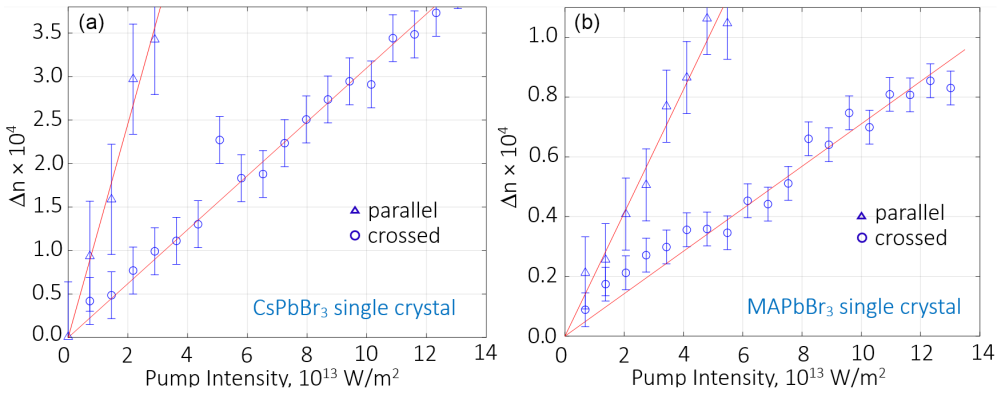

FIG. 4. Experimental Kerr-induced peak refractive index change Δn as a function of peak pump intensity for (a) $CsPbBr_3$, and (b) $MAPbBr_3$ for parallel and crossed polarization configurations. Nonlinear (Kerr) refractive index n_2 is found from fitting (red lines) as a coefficient of linear relation $\Delta n = n_2 I$.

reported Kerr index values in these compounds, which to the best of our knowledge were obtained by means of z-scan technique, we chose to measure n_2 by means of an alternative method. Namely, we have employed a direct interferometric pump-probe technique. Being a time-resolved alternative to the classic z-scan technique, it has a number of advantages, the most important one being that it can measure the instantaneous response of the medium while the z-scan works with a time-integrated signal. This distinction becomes important whenever extrinsic, nonelectronic channels of Kerr nonlinearity, such as photo-refractivity or heat-related phenomena, are characterized by long time-scales as compared to the repetition rate of the probing source.

Another advantage of the method adopted in this work is the less stringent requirements imposed upon the sample geometry as compared to z-scan, which allows us to measure n_2 in bulk single-crystal samples, thus minimizing the possible surface and size effects in the grains of polycrystalline samples. By analyzing the pump-induced phase shifts of the probe beam, we obtain $n_2 = +2.1 \times 10^{-14}$ cm^2/W for $CsPbBr_3$ and $n_2 = +0.6 \times 10^{-14}$ cm^2/W for $MAPbBr_3$. These numbers are significantly lower than the highest reported n_2 values in LHPs, on the other hand they are very reasonable for generic semiconductors with comparable electronic band gaps [31,32].

ACKNOWLEDGMENTS

We gratefully acknowledge the assistance of Prof. John Dudley.

[1] G. Findik, M. Biliroglu, D. Seyitliyev, J. Mendes, A. Barrette, H. Ardekani, L. Lei, Q. Dong, F. So, and K. Gundogdu, Nat. Photon. **15**, 676 (2021).
[2] A. Ferrando, J. P. M. Pastor, and I. Suárez, J. Phys. Chem. Lett. **9**, 5612 (2018).
[3] Y. Zhou, Y. Huang, X. Xu, Z. Fan, J. B. Khurgin, and Q. Xiong, Appl. Phys. Rev. **7**, 041313 (2020).
[4] J. Yi, L. Miao, J. Li, W. Hu, C. Zhao, and S. Wen, Opt. Mater. Express **7**, 3894 (2017).
[5] J. Serna, J. Uribe, E. Rueda, D. Ramirez, F. Jaramillo, J. Osorio, and H. García, Nonlinear optical properties of two and three-dimensional hybrid perovskite using single beam F-scan technique at 1064 nm, arXiv:1807.06703.
[6] R. Zhang, J. Fan, X. Zhang, H. Yu, H. Zhang, Y. Mai, T. Xu, J. Wang, and H. J. Snaith, ACS Photon. **3**, 371 (2016).
[7] B. S. Kalanoor, L. Gouda, R. Gottesman, S. Tirosh, E. Haltzi, A. Zaban, and Y. R. Tischler, ACS Photon. **3**, 361 (2016).
[8] K. N. Krishnakanth, S. Seth, A. Samanta, and S. V. Rao, Opt. Lett. **43**, 603 (2018).
[9] I. Suárez, M. Vallés-Pelarda, A. F. Gualdrón-Reyes, I. Mora-Seró, A. Ferrando, H. Michinel, J. R. Salgueiro, and J. P. M. Pastor, APL Mater. **7**, 041106 (2019).
[10] S. Mirershadi, S. Ahmadi-Kandjani, A. Zawadzka, H. Rouhbakhsh, and B. Sahraoui, Chem. Phys. Lett. **647**, 7 (2016).
[11] C. Kriso, M. Stein, T. Haeger, N. Pourdavoud, M. Gerhard, A. Rahimi-Iman, T. Riedl, and M. Koch, Opt. Lett. **45**, 2431 (2020).
[12] K. P. Goetz and Y. Vaynzof, ACS Energy Lett. **7**, 1750 (2022).
[13] M. Sheik-Bahae, A. Said, T.-H. Wei, D. Hagan, and E. V. Stryland, IEEE J. Quantum Electron. **26**, 760 (1990).
[14] P. B. Chapple, J. Staromlynska, J. A. Hermann, T. J. Mckay, and R. G. Mcduff, J. Nonlinear Opt. Phys. Mater. **06**, 251 (1997).
[15] R. de Nalda, R. del Coso, J. Requejo-Isidro, J. Olivares, A. Suarez-Garcia, J. Solis, and C. N. Afonso, J. Opt. Soc. Am. B **19**, 289 (2002).
[16] B. Chen, T. Li, Q. Dong, E. Mosconi, J. Song, Z. Chen, Y. Deng, Y. Liu, S. Ducharme, A. Gruverman, F. D. Angelis, and J. Huang, Nat. Mater. **17**, 1020 (2018).
[17] H. Tahara, T. Aharen, A. Wakamiya, and Y. Kanemitsu, Adv. Opt. Mater. **6**, 1701366 (2018).
[18] T. Handa, H. Tahara, T. Aharen, and Y. Kanemitsu, Sci. Adv. **5**, eaax0786 (2019).
[19] T. Haeger, R. Heiderhoff, and T. Riedl, J. Mater. Chem. C **8**, 14289 (2020).
[20] R. W. Boyd, *Nonlinear Optics*, 3rd edition (Academic Press, Burlington, 2008).
[21] T. Y. Chang, Opt. Eng. **20**, 220 (1981).
[22] A. Gnoli, L. Razzari, and M. Righini, Opt. Express **13**, 7976 (2005).
[23] M. I. Saidaminov, A. L. Abdelhady, B. Murali, E. Alarousu, V. M. Burlakov, W. Peng, I. Dursun, L. Wang, Y. He, G. Maculan, A. Goriely, T. Wu, O. F. Mohammed, and O. M. Bakr, Nat. Commun. **6**, 7586 (2015).
[24] M. I. Saidaminov, A. L. Abdelhady, G. Maculan, and O. M. Bakr, Chem. Commun. **51**, 17658 (2015).
[25] Y. Rakita, N. Kedem, S. Gupta, A. Sadhanala, V. Kalchenko, M. L. Böhm, M. Kulbak, R. H. Friend, D. Cahen, and G. Hodes, Cryst. Growth Des. **16**, 5717 (2016).
[26] G. Agrawal, *Nonlinear Fiber Optics* (Elsevier, Amsterdam, 2013).
[27] A. G. Volosniev, A. S. Kumar, D. Lorenc, Y. Ashourishokri, A. A. Zhumekenov, O. M. Bakr, M. Lemeshko, and Z. Alpichshev, Phys. Rev. Lett. **130**, 106901 (2023).
[28] Y. Wei, A. G. Volosniev, D. Lorenc, A. A. Zhumekenov, O. M. Bakr, M. Lemeshko, and Z. Alpichshev, J. Phys. Chem. Lett. **14**, 6309 (2023).
[29] G. Ermolaev, A. P. Pushkarev, A. Zhizhchenko, A. A. Kuchmizhak, I. Iorsh, I. Kruglov, A. Mazitov, A. Ishteev, K. Konstantinova, D. Saranin, A. Slavich, D. Stosic, E. S. Zhukova, G. Tselikov, A. D. Carlo, A. Arsenin, K. S. Novoselov, S. V. Makarov, and V. S. Volkov, Nano Lett. **23**, 2570 (2023).
[30] See Supplemental Material at http://link.aps.org/supplemental/10.1103/PhysRevMaterials.8.085403 for additional experimental details.
[31] M. Sheik-Bahae, D. J. Hagan, and E. W. V. Stryland, Phys. Rev. Lett. **65**, 96 (1990).
[32] M. Sheik-Bahae, D. Hutchings, D. Hagan, and E. V. Stryland, IEEE J. Quantum Electron. **27**, 1296 (1991).
[33] D. Lorenc and Z. Alpichshev, Appl. Phys. Lett. **123**, 091104 (2023).